

# Microporous Membranes of Polyoxymethylene from a Melt-Extrusion Process: (II) Effects of Thermal Annealing and Stretching on Porosity

MATTHEW B. JOHNSON, GARTH L. WILKES

Virginia Tech, Polymer Materials and Interfaces Laboratory and Department of Chemical Engineering, Blacksburg, Virginia 24061

Received 20 August 2001; accepted 7 September 2001

**ABSTRACT:** A two-part study utilizing polyoxymethylene (POM) was undertaken to investigate a three-stage process (melt-extrusion/annealing/uniaxial-stretching) utilized to produce microporous films. In this report, the thermal annealing (second stage) and subsequent uniaxial-stretching (third stage) results of selected POM films from two commercial resins, labeled D & F, are discussed. Specifically, the annealing and uniaxial stretching effects on film morphology, orientation, and other pertinent film properties are addressed. Additionally, sequential analysis was performed regarding the influence each stage had on the resulting microporosity. It was found that the melt-extruded precursor morphology and orientation, as a consequence of the first stage extrusion parameters and resin characteristics, are crucial to controlling the membrane permeability. The annealing parameters were also deemed critical, where a temperature of 145°C applied for 20 min under no tension was the optimum annealing condition for producing a highly microporous film upon stretching. For the conditions studied, the stretching parameters that were found to be optimum for producing the desired characteristics in the final film were a cold temperature of 50°C and hot stretch temperature of 100°C. The optimum extension levels were concluded to be 90% for both the cold and hot stretch steps, and thus a total overall extension level of 180%. However, these results were only with respect to resin F films. Because the resin D melt-extruded precursors possessed twisted lamellar morphologies and relatively low crystal orientation, their samples could not be produced into microporous films. © 2002 Wiley Periodicals, Inc. *J Appl Polym Sci* 84: 1762–1780, 2002; DOI 10.1002/app.10587

**Key words:** polyethylene; porosity; morphology; extrusion

## INTRODUCTION

This report describes the second portion of a two-part study regarding a process composed of three stages (Melt-Extrusion/Annealing/Uniaxial-Stretching) (MEAUS) utilized to make mi-

cro porous membranes. As discovered in our previous sequential investigation<sup>1,2</sup> of the MEAUS process where isotactic poly(4-methyl-1-pentene) (PMP) was utilized, the melt-flow behavior and its orientation prior to crystallization play critical roles in the formation of the morphological features and orientation of the crystallized film. From that study, it was concluded that a parallel planar stacked lamellar morphology possessing a relatively high crystalline orientation is the desirable structural features

---

Correspondence to: G. L. Wilkes (gwilkes@vt.edu).  
Contract grant sponsor: Celgard Corporation LLC.

*Journal of Applied Polymer Science*, Vol. 84, 1762–1780 (2002)  
© 2002 Wiley Periodicals, Inc.

for a melt-extruded precursor to possess. This type of lamellar arrangement is clearly a consequence of a row-nucleated morphology created by the appropriate melt-extrusion conditions.

In the first article of this two-part series,<sup>3</sup> the melt-extrusion results of three polyoxymethylene (POM) resins (D, E, and F) were reported. Resins D and E differed mainly in weight average molecular weight ( $M_w$ ) where resin D had a higher value, yet both resins were characterized by relatively narrow molecular weight distributions (MWD), ca. 1.6. In contrast, resin F possessed a broader MWD (ca. 6.8) but nearly the same  $M_w$  in comparison with resin D. Additionally, the broader MWD resin contained a small amount of ethylene oxide comonomer while the other resins did not contain comonomer. Upon controlled melt-extrusion, resin F precursors generally possessed parallel planar stacked lamellar textures, for the processing window considered. However, resin D or E samples were characterized by partially twisted lamellae that were arranged into oriented sheaf-like structures, and in some films, spherulitic-like morphologies predominated. Further, the crystalline orientation, as determined via wide-angle X-ray scattering (WAXS), was lowest for resin E specimens followed by those of resin D while resin F samples had the highest orientations. The results were attributed to the process conditions and melt-relaxation time differences (at a constant temperature) between resins, where resin F possessed the longest melt-relaxation time, followed by resin D and resin E, respectively.

The use of annealing (second stage) to promote structural modifications such as lamellar thickening and perfection in the melt-extruded precursor has also been considered important for the formation of microporous membranes made by the MEAUS process.<sup>2,4</sup> This has been accomplished through control of the annealing temperature ( $T_a$ ), annealing time ( $t_a$ ), and tension level (percent extension) during annealing. A requirement enabling crystal thickening and perfection is the occurrence of chain axis crystalline mobility. The thermal transition attributed to this is conventionally denoted as the  $\alpha_c$  relaxation.<sup>5,6</sup> As has been recognized, the existence of such a relaxation is "necessary, but not sufficient"<sup>7</sup> for lamellae to thicken, where the presence of noncrystallizable units along the polymer backbone (comonomer, branches, etc.), highly entangled interlamellar regions, and the nature of the mor-

phology may affect the crystalline thickening process. Indeed, the effect of comonomer on lamellae thickening will have important implications to this study as will be discussed later.

The presence of the  $\alpha_c$  relaxation is also believed to be important with respect to the third stage of the MEAUS process, i.e., uniaxial-stretching stage, which is composed of two uniaxial stretching steps followed by a thermal-relaxation/heat-setting step. The first stretching step is designated the "cold" stretch while the second is the "hot" stretch. The cold stretch temperature ( $T_{cs}$ ) generally occurs above the  $T_g$  but below the hot stretch temperature ( $T_{hs}$ ), which itself is below the annealing temperature of the prior stage but still in the upper temperature range of the  $\alpha_c$  relaxation. The extension levels utilized during the cold stretch (%CS) and hot stretch (%HS) steps also must be examined. The stretching directions in both steps are along the MD of the annealed film, i.e., perpendicular to the stacked lamellae. The cold stretch step is utilized to "nucleate" or initiate the micropores while hot stretching increases their overall pore size. It is in the latter step, hot stretching, that crystalline mobility is believed to enable greater extension levels and thus greater lamellar separation results if an  $\alpha_c$  relaxation exists. The thermal-relaxation/heat-setting step is utilized to allow partial recovery and impart dimensional stability to the film after removal from the stretching apparatus.

This sequential study of the MEAUS process addresses our findings with respect to POM. Although POM has been shown to form microporous films,<sup>8,9</sup> it has not been previously studied with the goal of producing microporous membranes. It is desired that the information obtained from this study will lend itself to understanding the formation of microporous materials via the MEAUS process. Additionally, the results are hoped to facilitate an improved working knowledge of the mechanisms behind each stage, i.e., melt-flow behavior during melt-extrusion, structural modifications occurring while thermal annealing, and the deformation processes taking place during stretching. This will be accomplished by consecutive analysis of the results from each of the three process stages. As stated earlier, the findings of the first stage (melt-extrusion) utilizing POM have already been presented.<sup>3</sup> In this second portion of the investigation, the annealing (second stage) and stretching (third stage) effects on POM film morphology, crystal orientation, and other

**Table I** Molecular Weight Characteristics for the Two POM Resins Studied

Resin	$M_n$ (kg/mol)	$M_w$ (kg/mol)	$M_w/M_n$	$T_m$ (°C)
D	78.5	125.8	1.60	178
F	19.2	130.9	6.82	167

pertinent properties are presented and discussed. Also, the same sample designation as utilized in part 1 will be employed for continuity. Specifically, in this report, we will address samples, D1, F1, F2, and F3, that were extruded under the conditions stated in Tables I and III3 from ref. 2. These POM melt-extruded precursor films were chosen based upon their morphological features and orientation state in order to investigate the effects of specific annealing ( $T_a$ ,  $t_a$ , and tension) and stretching process variables ( $T_{cs}$ , %CS,  $T_{hs}$ , and %HS).

## EXPERIMENTAL

### Materials

The precursor films from two resins (D & F) were utilized in this annealing and stretching investigation. Although the precursor films were in tubular form, these were split into strip form for the remaining two steps of the MEAUS process. The commercial resin D was a result of anionic polymerization of formaldehyde and end-capping the chains using acetic anhydride. The acetic anhydride was employed to stabilize the chain because POM has a relatively low ceiling temperature (ca. 120°C) and the chain undergoes depolymerization (unzipping) initiated at the hydroxyl end groups without end-capping. Resin F was polymerized via a ring-opening polymerization mechanism. This particular synthesis utilizes a small amount of the comonomer ethylene oxide to provide thermal stability to the POM chain. More information addressing the resin characteristics including molecular weight and its distribution is provided in Table I.

### Structural and Optical Techniques Utilized

#### Wide-Angle X-ray Scattering (WAXS)

WAXS studies were performed on a Philips tabletop X-ray generator model PW1720 equipped with a standard vacuum sealed Warhus photographic

pinhole camera. The X-ray beam was of Cu  $K\alpha$  radiation,  $\lambda = 1.544 \text{ \AA}$ , and was collimated to a beam diameter of 0.020 inches (0.508 mm).

As previously reported,<sup>3</sup> the extrusion is a planar extensional flow along the MD, which promotes uniaxial orientation behavior with respect to the MD axis. As a result, the nature of the crystalline orientation (orientation function) need only be obtained by examination of the azimuthal angle dependence of appropriate reflections arising from standard flat plate WAXS patterns. The orientation function utilized was the Hermans' orientation function ( $f_H$ ),<sup>11</sup>

$$f_H = \frac{(3 \cdot \overline{\cos^2\theta} - 1)}{2} \quad (1)$$

where  $\theta$  is the angle between the chain (or suitable specific unit cell axis) and a chosen reference axis, MD. The procedural details for determining the crystalline orientation ( $f_c$ ) in the POM films discussed in this article has been given in our first report.<sup>3</sup>

#### Small-Angle X-ray Scattering (SAXS)

SAXS was utilized to estimate the long spacing of the POM precursors. A slit collimation of dimensions  $0.03 \times 5 \text{ mm}$  was employed with a Kratky camera using nickel filtered Cu  $K\alpha$  radiation of wavelength 1.544 Å. The SAXS profiles were obtained by passing the beam along the normal direction (ND) to the film and obtaining the scan along the machine direction (MD). No desmearing of the slit-smear intensity data was undertaken in this investigation. After correction for parasitic scatter was performed using a Lupolen standard, the scattering curves were normalized to the incident intensity and sample thickness. This corrected intensity,  $I(\mathbf{s})$ , was plotted against the angular variable,

$$s = 2 \left( \sin \frac{\theta}{2} \right) / \lambda \quad (2)$$

where  $\theta$  is the radial scattering angle. The long period was estimated by using the eq. (1)  $\ell = 1/s^*$ , where  $s^*$  is the value of  $s$  at the first-order interference peak of the slit-smear  $I(s)$  vs.  $s$  plot. A "heterogeneity index" of the lamellar distribution in the structure was evaluated by determining the full peak width at half the maximum height ( $\Delta w$ ) of the first order scattering intensity peak.

**Table II** Pertinent Characteristics for the Melt-Extruded Films F1, F2, F3, and D1

Sample	Lamellar Morphology	$f_c$	$X_c$ (%)	$T_m$ (°C)	$\ell$ (Å)	$\Delta w$ (nm <sup>-1</sup> )
F1	Partially twisted	0.81	48	165	128	0.47
F2	Partially twisted	0.75	48	165	129	0.46
F3	Partially twisted	0.65	47	166	128	0.47
D1	Sheaf-like/twisted	0.45	52	178	153	0.51

### Atomic Force Microscopy (AFM)

AFM micrographs were obtained with the use of a Digital Instruments Nanoscope III Scanning Probe Microscope operated in TappingMode™. Nanosensor TESP single beam cantilever tips possessing force constants of  $35 \pm 7$  N/m and oscillated at frequencies of ca. 290 kHz were used. The films were placed upon glass slides using double stick tape with raster-scanning parallel to film MD.

### Differential Scanning Calorimetry (DSC)

DSC measurement was performed with a Perkin-Elmer DSC-7. Heating scans were conducted utilizing the procedures presented in our earlier report<sup>3</sup> that addressed melt extrusion of the precursor POM films and their characterization.

### Dynamic Mechanical Spectroscopy (DMS)

Dynamic mechanical testing was carried out on a Seiko DMS 210. The samples were tested in tensile mode using samples approximately 0.0254 mm thick, 10 mm long, 6 mm wide. The DMS experiments were performed at a frequency of 1 Hz using a heating rate of 2°C/min under a N<sub>2</sub> atmosphere.

### Gurley Instrument and Film Thickness

Film porosity was determined by measuring the stretched film permeability given in terms of the Gurley number, which is the time required for 10 cc of air to pass through the 1-inch square section of film at a constant pressure of 12.2 inches of H<sub>2</sub>O. The Gurley number measurements are performed using a Gurley densometer model No. 4150. Final films with measured Gurley values less than 100 s will be considered “quality” membranes. All Gurley numbers reported in this article arise from an average of a *minimum* of six measurements made for each sample. Film thickness measurements were carried out on a Series 400 Precision Micrometer.

## RESULTS

As already mentioned, four POM melt-extruded precursors, F1, F2, F3, and D1, were utilized for this study. All four films possessed stacked lamellar morphologies that were in some cases planar. Table II provides this information along with other pertinent film characteristics. Because the overall goal was to produce POM microporous film, the resin F films were the main focus in this report because these samples possessed planar lamellar morphologies and the highest  $f_c$  values of any POM films presented in the previous report.<sup>3</sup> However, the reader will recall that resin F also contained a very low mole percentage of the comonomer ethylene oxide while resins D and E did not. Thus, film D1 was selected for comparison purposes because it possessed the most planar lamellar morphology and highest  $f_c$  of any resin D or E sample. The comonomer effect can be seen in the lower  $T_m$ ,  $X_c$ , and SAXS long spacing ( $\ell$ ) of the resin F precursors relative to those of sample D1, as displayed in Table II.

### Annealing

Because of the large number of annealing and stretching variable combinations utilized, only selected results will be presented here that are, in general, representative of most POM films studied by the authors. The annealing temperatures utilized were chosen based upon the range of temperatures encompassing the POM mechanical  $\alpha_c$  relaxation, determined by DMA and expressed by  $\tan \delta$  in Figure 1. From this figure, the  $\alpha_c$  relaxation associated with the precursor F1 is observed to range from ca. 40 to 165°C while the temperature range is noted to be approximately 40–175°C for precursor D1. Annealing temperatures of 85, 110, 130, 145, and 150°C were employed for the resin F films while temperatures of 85, 120, 145, 155, and 160°C were used in the limited study of the resin D sample.

Annealing times of 5, 10, and 20 min were used in light of feasible industrial processing times and



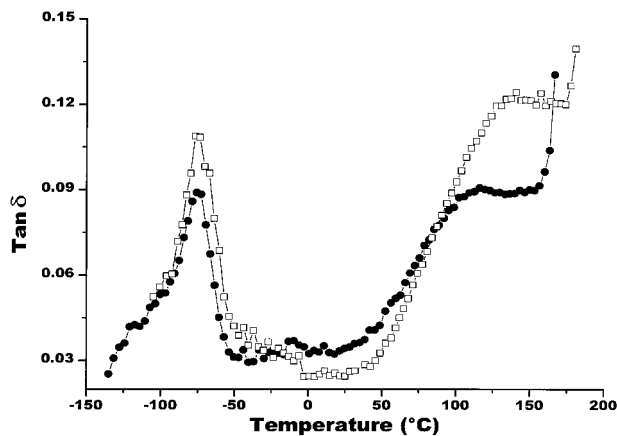


**Figure 1** Tan  $\delta$  as a function of temperature for POM films ( $\square$ ) D2 and ( $\bullet$ ) F2 with their corresponding  $\gamma$  and  $\alpha_c$  relaxations labeled. This data was obtained utilizing a heating rate of  $2^\circ\text{C}/\text{min}$  and a frequency of 1.0 Hz.

to provide continuity with our previous MEAUS investigation of PMP.<sup>2</sup> The final annealing variable investigated was the tension level (percent extension) applied to the film. The tension (elongation) level was divided into two main categories: annealing without tension (free-anneal or 0% tension) and annealing under a specified tension level. In the case of the latter, the tension levels were 3, 9, and 15%. The specific level was applied during the annealing stage with a small mechanical stretching apparatus that was also employed in the stretching stage. The specific levels of 3, 9, and 15% tension were based upon the previous work of Yu<sup>12</sup> on linear high density polyethylene (HDPE) films and our investigations of PMP films.<sup>1,2</sup> As mentioned, the utility of the annealing stage in the MEAUS process is to produce structural changes within the precursor film as a function of annealing temperature, time, and tension level. In Figure 2 it is recognized that the first-order SAXS peak shifted to lower values of  $s$  as the annealing temperature was increased, and thus the long spacing ( $\ell$ ) increased relative to the precursor. These long spacing results clearly show that the average lamellar thickness increased upon annealing relative to the precursor. It is further observed in this figure, that the peak width at half the maximum ( $\Delta w$ ) decreased with annealing. This result regarding  $\Delta w$  suggests that the lamellar distribution has become more uniform upon annealing. Also note that, as the specific annealing temperature was increased, the crystalline phase thickened (i.e.,  $s^*$  is smaller than the  $s^*$  value characterizing the precursor)

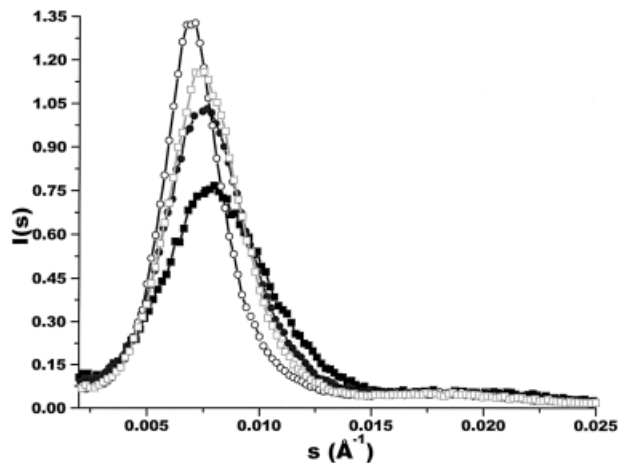


**Figure 2** Slit-smear intensity for precursor F1 and F1 free-annealed films as a function of annealing temperature for  $t_a = 20$  min: ( $\blacksquare$ ) precursor, ( $\bullet$ )  $T_a = 110^\circ\text{C}$ , ( $\square$ )  $T_a = 130^\circ\text{C}$ , ( $\circ$ )  $T_a = 145^\circ\text{C}$ .

and was more uniform in thickness (i.e.,  $\Delta w$  decreases vs. the precursor). The annealing temperature effects just described held for all the resin F films and are plotted as a function of annealing time in Figure 3 for  $\ell$  and in Figure 4 for  $\Delta w$ . Upon examination of these figures, when annealing a resin F film, it is recognized that as the annealing time or temperature increased, the lamellar thickness generally increased while  $\Delta w$  decreased.

Figure 5 presents the slit-smear SAXS profiles of four D1 free-annealed films with different annealing temperatures ( $t_a = 20$  min) and the

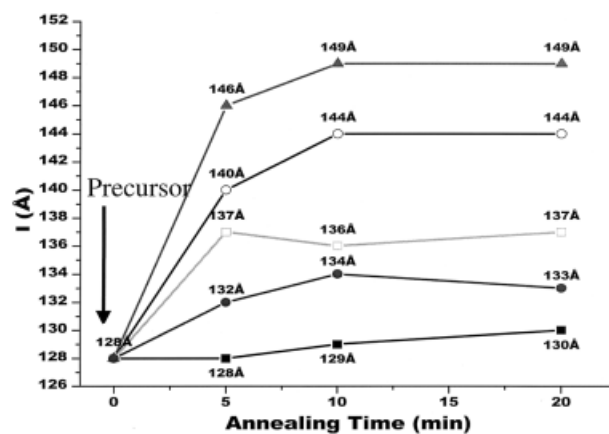


**Figure 3** Long spacing ( $\ell$ ) for free-annealed F1 films as a function of annealing time (x-axis) and temperature: ( $\blacksquare$ )  $T_a = 85^\circ\text{C}$ , ( $\bullet$ )  $T_a = 110^\circ\text{C}$ , ( $\square$ )  $T_a = 130^\circ\text{C}$ , ( $\circ$ )  $T_a = 145^\circ\text{C}$ , and ( $\blacktriangle$ )  $T_a = 150^\circ\text{C}$ .

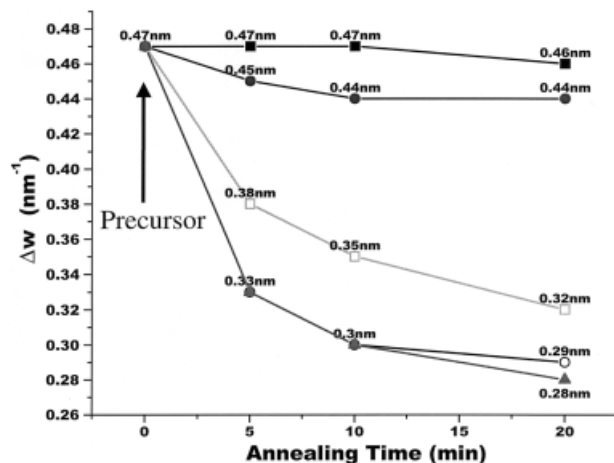


**Figure 4** Full width at half the maximum of the first-order slit-smear SAXS peak for free-annealed F1 films as a function of annealing time (x-axis) and temperature: (■)  $T_a = 85^\circ\text{C}$ , (●)  $T_a = 110^\circ\text{C}$ , (□)  $T_a = 130^\circ\text{C}$ , (○)  $T_a = 145^\circ\text{C}$ , and (▲)  $T_a = 150^\circ\text{C}$ .

corresponding precursor. In this figure, it is clear that, for the annealing temperatures utilized, lamellar thickening occurred upon annealing the precursor D1. These annealed D1 film results are also tabulated in Table III. It is recognized that the magnitude of the calculated long spacing values for the D1 free-annealed films are much larger than those of the F1 free-annealed films for equal conditions. For example, the D1 film free-annealed at  $145^\circ\text{C}$  for 20 min was found to possess a long spacing of  $181 \text{ \AA}$  while the comparably annealed F1 film was characterized by a value of only  $144 \text{ \AA}$ . It is reiterated that resin F contains ethylene oxide as a comonomer while resin D contains no comonomer. It is also recognized in Figure 5 that weak second-order interference peaks are present for each sample. Additionally, note that the data displayed in Figure 5 is slit-smear, and thus the first- and second-order peaks are not as prominent (intense) or narrow as they would be if desmearing had been undertaken.

The effect of annealing temperature on the melting endotherm of resin F free-annealed films is displayed in Figure 6. It is observed that the DSC trace was not significantly affected by annealing the film at  $110^\circ\text{C}$  relative to the trace of the precursor. However, the F1 films annealed at either  $145$  or  $150^\circ\text{C}$  are characterized by sharper melting profiles shifted to slightly higher temperatures relative to the precursor. Figure 7 shows the dependence of  $T_m$  and  $X_c$  on annealing tem-

perature and time for the F1 free-annealed films. It is found that  $T_m$  is *not* systematically shifted to higher temperatures for either annealing temperature ( $110$  or  $145^\circ\text{C}$ ). In contrast, as annealing time and/or temperature increased, so did  $X_c$  for these F1 free-annealed specimens, albeit marginally at the lower temperature of  $110^\circ\text{C}$ . These findings, along with other pertinent annealing results, are displayed in Table IV for the F1 films. Although not shown, the D1 films when annealed responded similarly, i.e.,  $X_c$  was systematically affected by annealing temperature and/or time while  $T_m$  was not.

Figure 8(a) and (b) display the effect annealing temperature ( $110$  or  $145^\circ\text{C}$ , respectively) had on the morphology of free-annealed F1 films. It is evident there are not any noticeable differences between these micrographs. In Figure 9(a)–(d), AFM micrographs are presented of F1 annealed films where tension was applied during annealing at a temperature of  $110$  or  $145^\circ\text{C}$ . At lower levels (3%), regardless of annealing temperature [Fig. 9(a) and (b)], tension does not visibly alter the morphology. However, lamellar deformation is observed for F1 films annealed under higher tension levels (15%) at  $145$  and  $110^\circ\text{C}$  for 20 min [Fig. 9(c) and (d), respectively]. The structural changes displayed in these latter two figures are different from each other. Specifically, for the sample annealed at  $145^\circ\text{C}$  [Fig. 9(c)], the lamellae appear to be oriented at an angle to the MD or draw direction. In Figure 9(d), void containing morphologies, indicated by arrows, are apparent in this

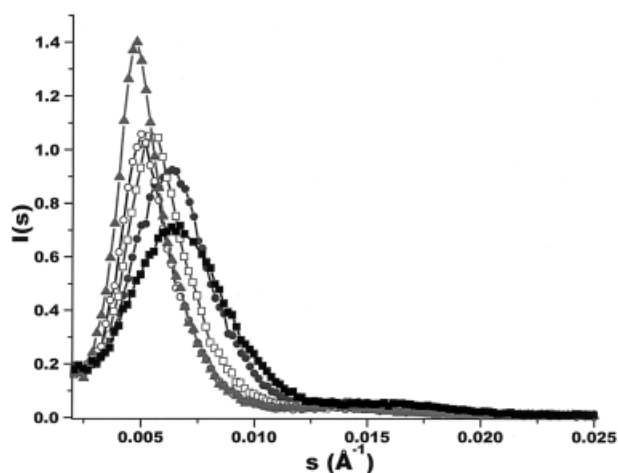


**Figure 5** Slit-smear intensity for precursor D1 and D1 free-annealed films as a function of annealing temperature for  $t_a = 20$  min: (■) precursor, (●)  $T_a = 120^\circ\text{C}$ , (□)  $T_a = 145^\circ\text{C}$ , (○)  $T_a = 155^\circ\text{C}$ , and (▲)  $T_a = 160^\circ\text{C}$ .

**Table III** Pertinent Film Characteristics of Selected D1 Annealed Films

$T_a$ (°C)	precursor	85	120	145	155	160
$t_a$ (min)	—	20	20	20	20	20
% tension	—	free	free	free	free	free
$\ell$ (Å)	153	155	162	181	200	208
$\Delta w$ (nm <sup>-1</sup> )	0.49	0.43	0.39	0.30	0.25	0.21

film annealed at a lower temperature (110°C). The presence of voids for the sample presented in Figure 9(d), promoted greater turbidity (haze) than the samples in Figures 8 and 9(a)—(c). In fact, given a specific annealing temperature, the film annealed with the greater level of tension visually displayed a greater level of turbidity. Additionally, for a tension level greater than 3%, the sample annealed at a lower temperature visually possessed a greater haze than the film annealed at a higher temperature. Although not presented here, these optical results were independent of annealing time for the processing window studied. An increased turbidity is accounted for by an increase in void content because the voids induced by tension increase the number of interfaces within the film, and as a result a greater fraction of the incident light is scattered and/or reflected. The development of voids with increasing tension is also supported by the slit-smear SAXS data, as displayed in Figure 10(a) and (b), for a number of the same films presented in Figures 8 and 9. In the case of Figure 10(a), the SAXS profiles are provided for each sample annealed at

a lower tension level ( $\leq 3\%$ ). Each profile displays a first-order scattering peak with a value of  $s^*$  consistent with that determined for the comparably free-annealed specimens. In other words, the long spacing values obtained for the annealed samples, when the tension was lower ( $\leq 3\%$ ), were only dependent upon the temperature or time of annealing. Further, the sample annealed at the higher temperature (145°C) under 15% tension is characterized by a value of  $s^*$  similar to the sample annealed at the same temperature but a lower tension level (i.e.,  $T_a = 145$  at 3% tension). The scattering profiles of these two films differ only in the peak intensity  $[I(s)]$ , where the higher the tension level, the lower the value of  $I(s)$ . The inserted figure labeled (b) in Figure 10 provides the complete data, but rescaled in intensity, for the samples annealed at 110°C for either 5 or 20 min under a tension of 15%. It is noted that these samples possess a much higher peak intensity relative to those annealed at 145°C, and are also characterized by a much lower value of  $s^*$ . In fact, the value of  $s^*$  is associated with a long spacing

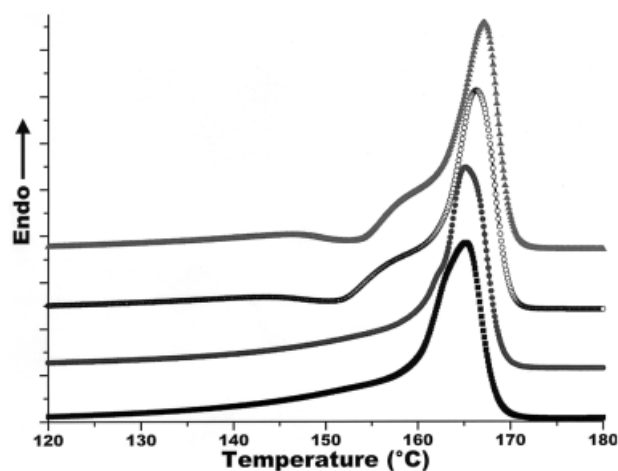


**Figure 6** DSC heating scans of the F1 precursor and F1 free-annealed films for  $t_a = 20$  min: (■) precursor, (●)  $T_a = 110^\circ\text{C}$ , (○)  $T_a = 145^\circ\text{C}$ , and (▲)  $T_a = 150^\circ\text{C}$  utilizing a heating rate of  $30^\circ\text{C}/\text{min}$ .

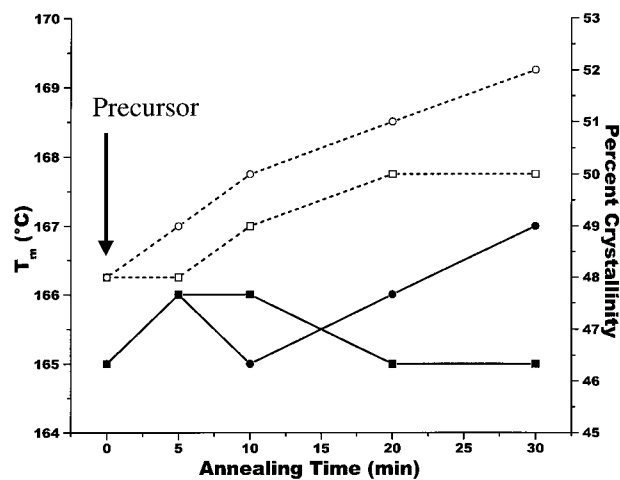


**Figure 7** The  $T_m$  (solid lines and solid data points) and  $X_c$  (dashed lines and open data points) results for the F1 precursor and selected F1 free-annealed films as a function of  $t_a$ : (■) and (□)  $T_a = 110^\circ\text{C}$ , (●) and (○)  $T_a = 145^\circ\text{C}$ .

**Table IV Pertinent Annealed F1 Film Properties at Different  $t_a$  (min),  $T_a$  (°C), and Percent Tension Combinations**

$T_a$ (°C)	$t_a$ (min)	% Tension	$T_m$ (°C)	$X_c$ (%)	$f_c$
110	5	free	166	48	0.81
110	20	free	165	50	0.81
110	20	3%	167	50	0.81
110	20	15%	166	50	0.76
130	5	free	166	48	0.81
130	20	free	165	50	0.81
145	5	free	166	49	0.81
145	20	free	166	51	0.81
145	20	3%	168	51	0.80
145	20	9%	167	51	0.75
145	20	15%	166	51	0.69
150	5	free	166	50	0.81
150	20	free	167	52	0.81

equal to approximately 14 nm. It is also recognized that this finding is independent of the annealing time used. The authors note that the above SAXS, DSC, and AFM findings as well as the optical observations were found to occur for all resin F films.

The reader will recall from Table IV that there was also an effect of tension during annealing on the crystal “c”-axis orientation ( $f_c$ ). Specifically, the orientation unexpectedly decreased as the specific tension level utilized increased above 3%. For a specific tension level of 3% or greater, the orientation also generally decreased as the isothermal annealing temperature increased (e.g., 110 vs. 145°C). Thus, a film annealed at 110°C for 20 min under 15% tension possessed a lower  $f_c$  than a film annealed at 145°C when all other MEAUS variables were held constant. This lower orientation (WAXS) occurred when the tension level or annealing temperature increased as long as the tension was greater than 3%. It is the (100) reflection that is used to calculate  $f_a$ , which also then allows one to calculate  $f_c$  as described previously.<sup>3</sup> Although not shown here, the value of  $f_c$  was unaffected by annealing time.

Figure 11(a)–(d) displays the WAXS patterns obtained for selected F3 annealed films with the X-ray beam along the film ND. These photographs are of annealed films from the precursor F3 where different tension levels (0 or free, 3, 9, and 15%) were applied at a temperature of 145°C for 20 min. The  $f_c$  values corresponding to the films represented in Fig. 11(a)–(d) are ca. 0.63, 0.61, 0.55, and 0.44, respectively. It is also apparent in these WAXS photographs that the *meri-*

*donal* intensity of the (100) reflection, due to some “a”-axis orientation, is observably more intense for the sample annealed at 3% tension than for any other presented. As the tension level was further increased to 9%, the meridonal reflection disappeared, and was totally absent for the sample annealed with 15% tension. Although the precursor photograph is not shown here, it was similar to the WAXS pattern for the free-annealed film. These results were independent of annealing time. As previously reported,<sup>3</sup> the F1 precursor displayed little “a”-axis orientation, as indicated by its WAXS pattern. The same trend just described of an axis orientation and its correlation to tension level, however, occurred for all resin F films.

### Stretching

The annealed films were subjected to the two-step uniaxial stretching process briefly described earlier in this report. Besides crosshead speed, which was kept constant throughout the entire study at 150 mm/min, there were two main variables to be accounted for in each stretching step. The first was temperature (cold stretch and hot stretch temperature), and the second was the percent extension the film was subjected during each step. The cold stretch temperatures studied were 25, 35, 50, and 70°C while the extension levels utilized were 50, 70, and 90%. The hot stretching temperatures ( $T_{hs}$ ) utilized were 85, 100, 115, 130, and 145°C with levels of extension (%HS) of 50, 65, 80, and 90%. The levels of extension were calculated using eq. (3):



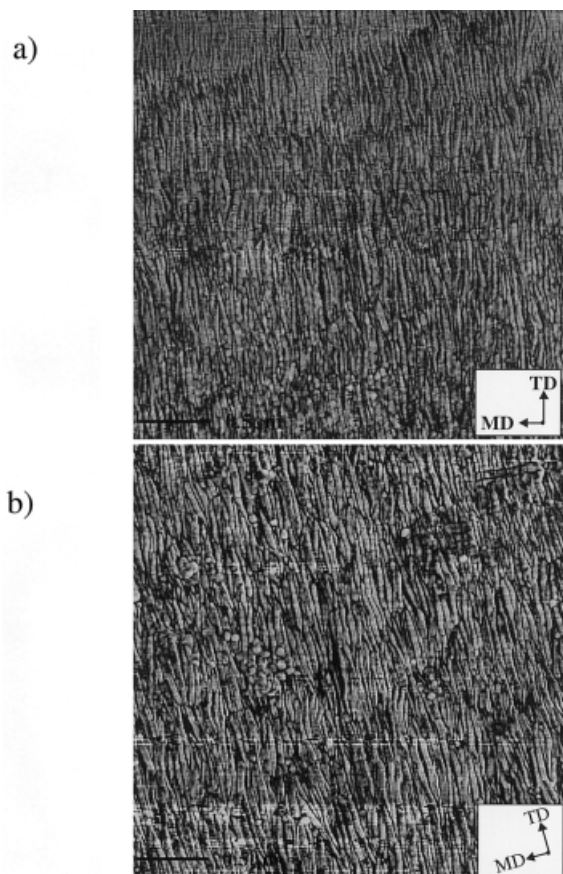


**Figure 8** AFM images of F1 films free-annealed for 20 min (a)  $T_a = 145^\circ\text{C}$ , and (b)  $T_a = 110^\circ\text{C}$ . The MD is labeled. Phase images are each  $3 \times 3 \mu\text{m}$ .

$$\% \text{ Extension} = \frac{l_f - l_o}{l_o} \times 100\% \quad (3)$$

where  $l_f$  is the final length of the film after the cold stretch or hot stretch step, and  $l_o$  is the initial length of the film *prior to any cold stretching*.

For this investigation, the film was not allowed to relax after stretching. This is due to the adverse affects relaxation was found to have on film permeability.<sup>2</sup> A heat-setting step was employed for *all* films having undergone the stretching stage. This was done so that the film retains approximately the same dimensions after removal from the stretching device. The heat-setting step occurred immediately after hot stretching in the same oven at the same hot stretch temperature for a period ca. 10 min.

From the above, it is clear that the possible number of annealing/stretching combinations is large, but the authors do not want to give the impression that every combination was at-

tempted. Instead, the samples reported here will represent the general findings and will be based on a “standard” set of annealing and stretching conditions. Any variation(s) from these conditions will be noted. These standard conditions consisted of a film free-annealed at  $145^\circ\text{C}$  for 20 min, followed by cold stretching at  $50^\circ\text{C}$  to 50% extension, then hot stretching at  $100^\circ\text{C}$  to an extension level of 90%. Heat setting occurred at the hot stretching temperature for 10 min. When any variation was made to this standard stretching condition, the remaining parameters were *not* altered, unless otherwise noted. Thus, a simple sample nomenclature was developed to track the sample history in this annealing/stretching process. This nomenclature designates the final film based upon its precursor and the particular variable(s) that was altered. For example, if a F1 film was annealed at  $85^\circ\text{C}$  instead of  $145^\circ\text{C}$ , following stretching, the final sample would be labeled F1- $T_a85$ . The remaining annealing and stretching conditions would be analogous to the standard conditions given above.

The effects of annealing on the structure and morphology are addressed first regarding their influence on microporosity after stretching. The Gurley number dependence on annealing temperature is shown in Figure 12 for stretched films from the precursors F1 and F2. The Gurley number, inversely related to permeability and porosity, was found within error to decrease as the isothermal annealing temperature increased to  $145^\circ\text{C}$  where the lowest Gurley value was obtained. However, film permeability increased as the annealing temperature was increased to  $150^\circ\text{C}$ . This trend occurred for both sample series F1 and F2 with the F1 membranes possessing higher permeability than the F2 counterparts. The reader may recall that the F1 precursor possessed a higher  $f_c$  than did the F2 precursor. A suitable or “quality” porous membrane is defined here as one possessing a Gurley number of 100 s or less. Within error, all the F1 final film results in “quality” membranes, but there are not any “quality” Gurley numbers for the F2 samples presented in this figure.

Figure 13(a)–(d) presents the morphologies, as obtained via AFM, corresponding to some of the results within Figure 12. Figure 13(b) and (d) each display an image of the F1 film prepared using the standard condition. The latter of these is of a higher magnification image for better observation of one of the membrane’s finer structure. Figure 13(a), which is of film F1- $T_a110\text{C}$ ,

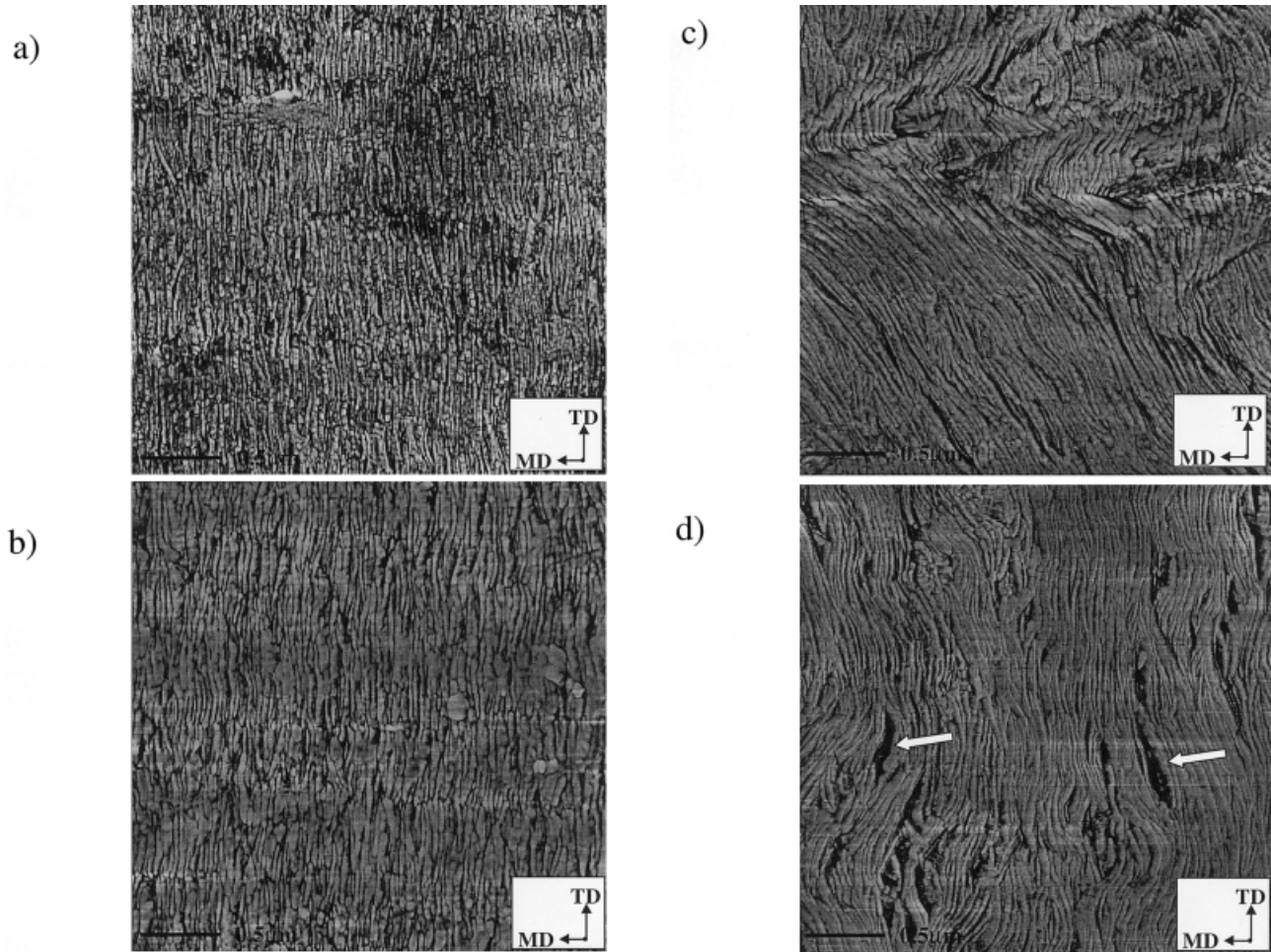


**Figure 9** AFM phase images of F1 films annealed for 20 min under tension (a) 3% tension,  $T_a = 145^\circ\text{C}$ ; (b) 3%,  $110^\circ\text{C}$ ; (c) 15%,  $145^\circ\text{C}$ ; and (d) 15%,  $T_a = 110^\circ\text{C}$ . The MD is labeled. Images are each  $3 \times 3 \mu\text{m}$ .

possesses less numerous and smaller micropores than the other two films annealed at higher temperatures. The authors have noted that most POM microporous membranes have an appearance that is somewhat different than those of the HDPE,<sup>12</sup> isotactic polypropylene,<sup>13</sup> or PMP<sup>2</sup> polyolefin films known to produce micropores. Specifically, the lamellae individually splay apart in the POM membranes while the specified polyolefin films tend to possess many lamellar bundles or “islands” between micropores. Additionally, the micropores are not as large in the POM final films as those in the polyolefin stretched samples. It is, however, recognized that both polyolefin and POM microporous membranes are characterized by bundles of tie-chains between lamellae oriented parallel to the stretch direction (MD).

Annealing time also influenced microporosity as measured via Gurley number with supporting

data given in Figure 14. In this figure, the Gurley values are a function of annealing time for stretched films from both precursors F1 and F2. As the annealing time was increased, the film permeability distinctly increased. Again, the F1 stretched films are characterized by higher porosity than the F2 materials for equal conditions.

The application of tension during annealing was shown earlier in this report to alter the annealed film morphology, and thus it was expected to impact the microporous structure and permeability of the final film. Data supporting this statement is given in Figure 15 for both F1 and F2 films. In either film series, higher tension levels (percent extension) during annealing yield higher Gurley numbers following stretching. In fact, films annealed with 15% tension possessed essentially nonporous properties as indicated by a Gurley value greater than 1000 s. This result was



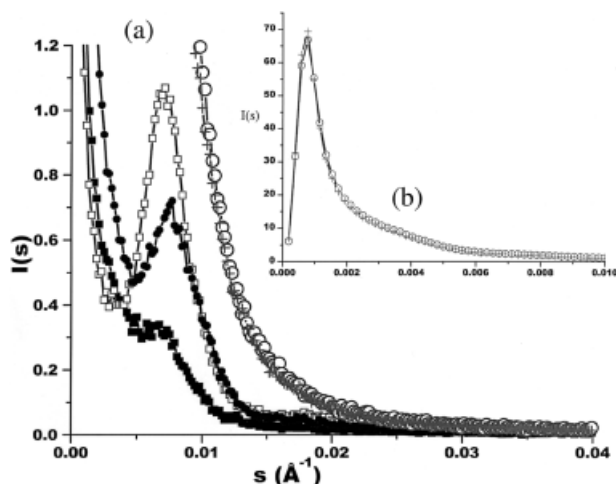


**Figure 10** Slit-smear intensity for F1 annealed films under tension (i) (■)  $T_a = 145^\circ\text{C}$ ,  $t_a = 20$  min, 15% tension; (ii) (□)  $T_a = 145^\circ\text{C}$ ,  $t_a = 20$  min, 3% tension; (iii) (○)  $T_a = 110^\circ\text{C}$ ,  $t_a = 20$  min, 15% tension; (iv) (+)  $T_a = 110^\circ\text{C}$ ,  $t_a = 5$  min, 15% tension; (●)  $T_a = 110^\circ\text{C}$ ,  $t_a = 20$  min, 3% tension. The inset (b) provides a rescaling of the data for plots (iii) and (iv).

regardless of the resin F precursor used. However, some “quality” membranes were obtained from both film series. The effect of tension during annealing on the stretched film microporous structure for films F1-3%tension and F1-9%tension is shown via AFM in Figure 16(a) and (b), respectively. For comparison, these micrographs should be contrasted against a membrane produced using the standard condition [recall Fig. 13(d)]. Clearly, the microporous character was eliminated as the tension level increased. These morphological results are somewhat expected based upon the Gurley numbers previously discussed. In summary of the annealing effects, the Gurley value, the stretched film thickness, and the normalized Gurley number to film thickness values are presented in Table V for a number of F1 membranes. The Gurley numbers normalized on film thickness, which are more accurate values for membrane comparison, again well verify the trends regarding the influence of the annealing conditions on the stretched films discussed above.

We now address the uniaxial-stretching stage of the MEAUS process with the presentation of the cold-stretching results. Because it has been established that the permeability (as related to Gurley) of the F2 films parallel the trends of F1 membranes, only the stretching results from the precursor F1 will be given. Figure 17 is a plot of the Gurley values as a function of both the per-

cent cold stretch extension (x-axis) and stretching temperature for F1 membranes. It is apparent that as the extension was increased, the Gurley number decreased. The lowest Gurley value occurred for the film cold stretched to 90% at a temperature of  $50^\circ\text{C}$ . Membranes produced using this cold stretch temperature ( $50^\circ\text{C}$ ) possessed the highest porosity followed by those final films cold stretched at temperatures of 70 and  $35^\circ\text{C}$ , respectively, for comparable annealing and stretching conditions. These Gurley values along with others that resulted from different cold stretch variable combinations are presented in Table VI. The trends described above still existed for the normalized results, although this data is not presented here.

The influence of the hot stretching parameters on membrane permeability is shown in Figure 18. Table VII presents all the membrane Gurley values that are a result of a number of additional hot stretch variable combinations with the remainder of the standard conditions intact. The figure displays the expected results concerning the percent hot stretch and its influence on permeability; as the percent hot stretch extension increases, so

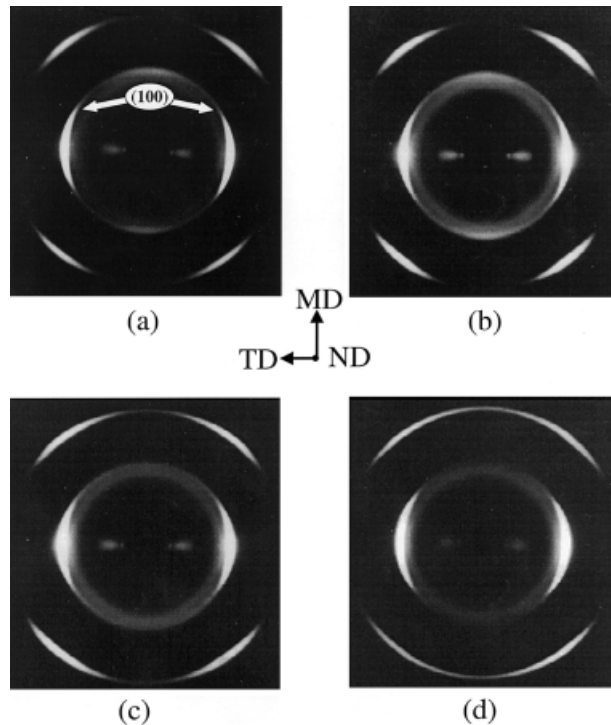


**Figure 11** WAXS photographs of the F2 annealed films with tension where  $T_a = 145^\circ\text{C}$  for  $t_a = 20$  min: (a) free annealed, (b) 3% tension, (c) 9% tension, and (d) 15% tension. The MD is labeled.

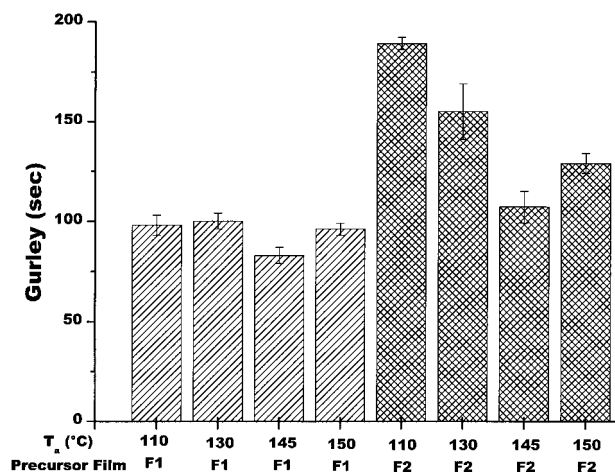


**Figure 12** Effect of annealing temperature on the Gurley number for F1 and F2 stretched films with the remainder of the main anneal/stretching condition kept intact.

does permeability. It was also found that the temperature at which hot stretching occurs affected the Gurley values in the following manner. As the temperature was increased from 85 to 100°C, permeability increased; however, further increasing the temperature above 100°C produced a decrease in permeability. In fact, at a hot stretch temperature of 145°C, which is equal to the standard annealing temperature, the films were impermeable. This is especially apparent upon observing the morphology of this film as shown in Figure 19. This lack of porosity occurred for any membrane that was hot stretched at a temperature equal to or greater than its annealing temperature (i.e.,  $T_{hs} > T_a$ ). Although the normalized Gurley values are not presented here, the data trends just described were not different.

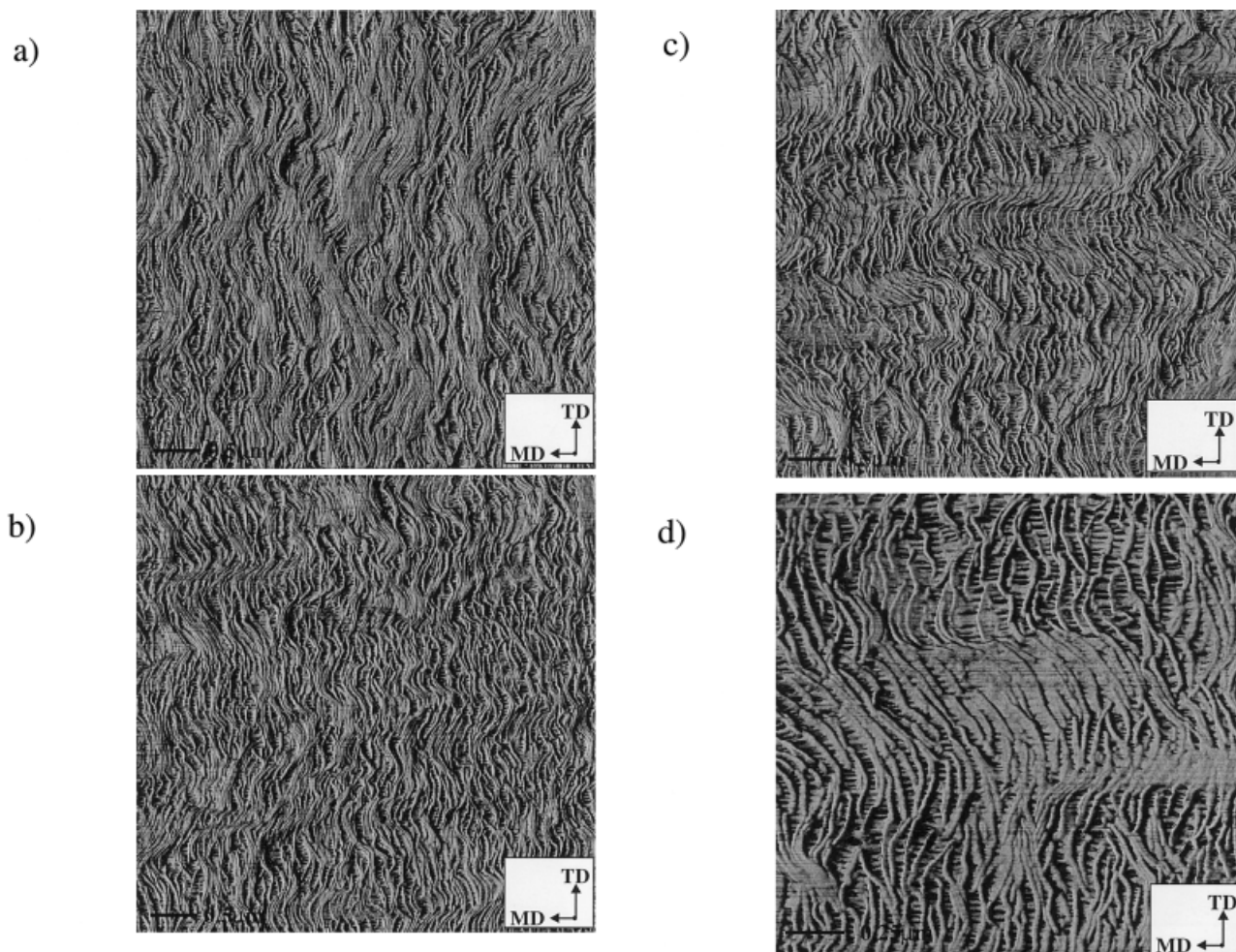


**Figure 13** AFM phase images of the resin F POM stretched films: (a) F1- $T_a$ 110C, (b) F1- $T_a$ 145C (standard condition), (c) F1- $T_a$ 150C, and (d)  $2 \times 2 \mu\text{m}$  image of (b). The MD is labeled. Images are each  $5 \times 5 \mu\text{m}$  except for (d).



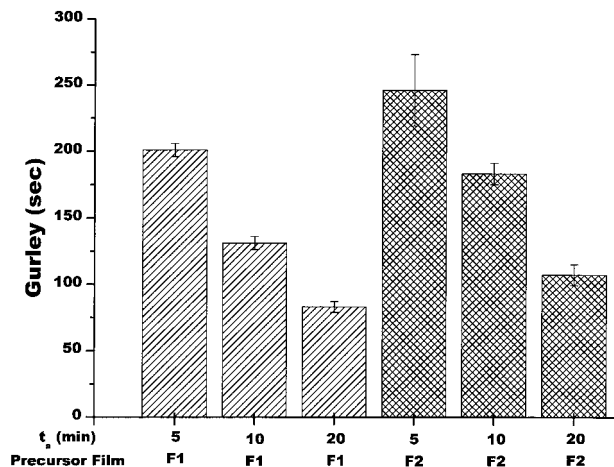


**Figure 14** Effect of annealing time on the Gurley number for F1 and F2 stretched films with the number of the main anneal/stretching condition kept intact.

If the Gurley value is plotted as a function of the total stretch, similar results to Figures 16 or 17 are observed—the reader only need to sum up the percent cold and hot stretch. In doing so, the total stretch values expressed in Figure 16 are 140, 160, and 180%, while those for Figure 17 are 100, 115, 130, and 140%. The Gurley numbers corresponding to the stretched films with their total extension values are displayed in Table VIII along with other cold and hot stretch combinations (the %TS values for the respective films are tallied in the top left corner of each cell). With one exception, the F1 membranes presented in this table are characterized as “quality” microporous

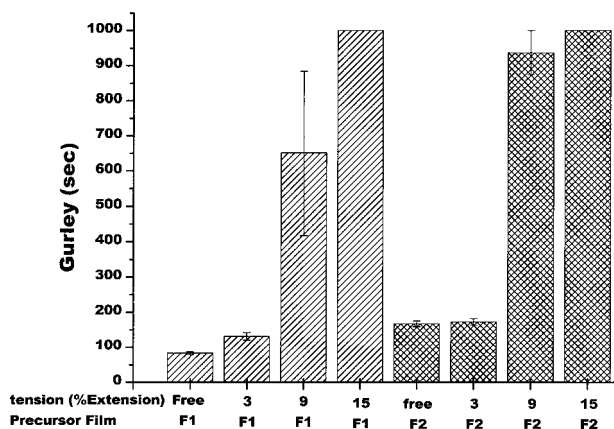


**Figure 15** Effect of tension level during annealing on the Gurley number for F1 and F2 stretched films with the remainder of the main anneal/stretching condition kept intact.

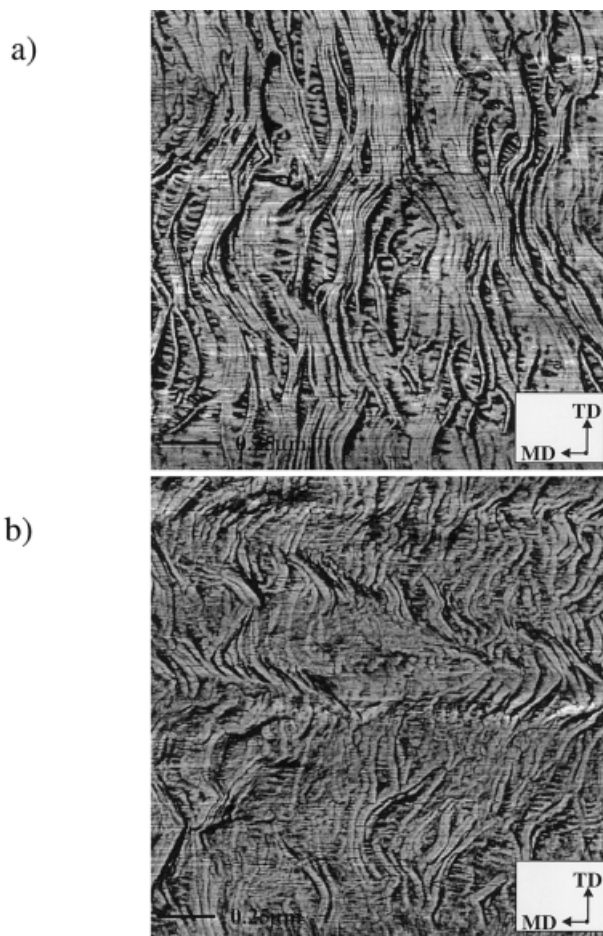


**Figure 16** AFM images of the resin F POM stretched films displaying the effect of tension during annealing on the microporosity: (a) 3% tension, and (b) 9% tension. The MD is labeled. The images are each  $2 \times 2 \mu\text{m}$ .

films. The reader may recall that as the percent cold stretch (or %HS) increased for a constant hot stretch (or %CS), a lower Gurley number resulted. Thus, it was expected and indeed realized that the lowest Gurley values occurred for stretched films where both parameters (%CS & %HS) were maximized. The effect on morphology, as viewed by AFM, is shown for the two extremes of 100 and 180% total stretch in Figure 20(a) and (b), respectively. Clearly, there is an observable difference in pore size between the two films, as measured along the MD, where the film produced with the larger total stretch is characterized by a larger pore size. Note that the micrograph displayed in Figure 20(b) is the microporous morphology for the F1 film possessing the lowest Gurley (highest porosity) of any film prepared during this study.

**Table V Pertinent Annealed F1 Film Properties at Different  $t_a$  (min),  $T_a$  (°C), and Percent Tension Combinations, Where All Other Annealing/Stretching Parameters Remained Constant with the Standard Condition**

$T_a$ (°C)	$t_a$ (min)	Tension (% Exten.)	Gurley (s)	Film Thickness (mil)	Norm. Gurley (s/mil)
110	20	free	98 ± 5	0.76	129
110	20	3%	215 ± 21	0.74	290
110	20	15%	≥1000	—	—
130	5	free	223 ± 22	0.76	293
130	20	free	100 ± 4	0.76	132
145	5	free	201 ± 5	0.75	268
145	20	free	83 ± 4	0.78	106
145	20	3%	131 ± 11	0.76	172
145	20	9%	651 ± 233	0.73	892
145	20	15%	≥1000	—	—
150	5	free	125 ± 15	0.75	167
150	20	free	96 ± 3	0.73	132

In a similar manner to the resin F films, precursor D1 was annealed and stretched using different parameter combinations. However, the resulting morphology and permeability were, as expected, dramatically different due to differences in the starting precursor morphology and crystalline orientation. Figure 21 provides an AFM micrograph of a D1 final stretched sample produced using the standard annealing/stretching conditions. It is evident that this D1 stretched film is absent of *any* microporous structure and analogous results were observed for *all* other annealing

and stretching combinations concerning the resin D films. Thus, no further results addressing the resin D stretched films will be presented.

## DISCUSSION

The annealing results presented displayed that many physical properties of the annealed film including morphology, lamellar thickness, and its distribution (as related to long spacing), and the degree of crystallinity ( $X_c$ ) are controlled to varying degrees by the annealing temperature ( $T_a$ ), time ( $t_a$ ), and tension level. The application of

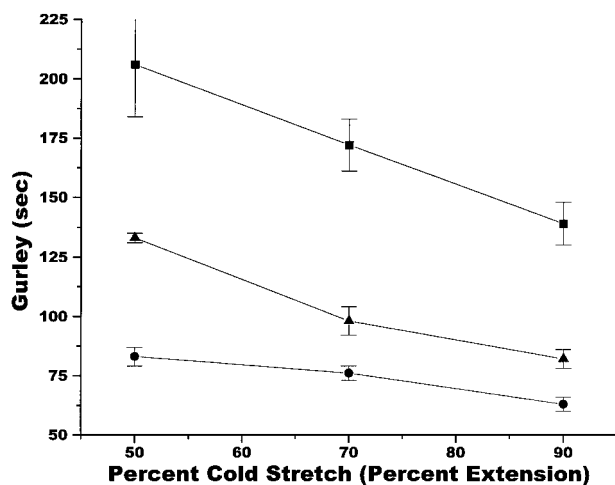


**Figure 17** Effect of the cold stretch parameters ( $T_{cs}$  and %CS) on the Gurley number for F1 stretched films with the remainder of the main anneal/stretching condition kept intact (■)  $T_{ca} = 35^\circ\text{C}$ , (●)  $T_{ca} = 50^\circ\text{C}$ , and (▲)  $T_{ca} = 70^\circ\text{C}$ .

**Table VI The Gurley Number Results from Membranes of Different %CS and  $T_{cs}$  Combinations: All-Other Annealing/Stretching Parameters Remained Constant with the Standard Condition**

$T_{cs}$ (°C)	% CS (% Extension)		
	50	70	90
25	423 ± 24 s	NP <sup>a</sup>	NA <sup>b</sup>
35	206 ± 22 s	172 ± 11 s	139 ± 9 s
50	83 ± 4 s	76 ± 3 s	63 ± 3 s
70	133 ± 2 s	98 ± 6 s	82 ± 4 s

<sup>a</sup> NP denotes a sample that was not produced because sample rupture occurred repeatedly for a number of attempts during cold stretching.

<sup>b</sup> NA denotes a variable combination that was not attempted.

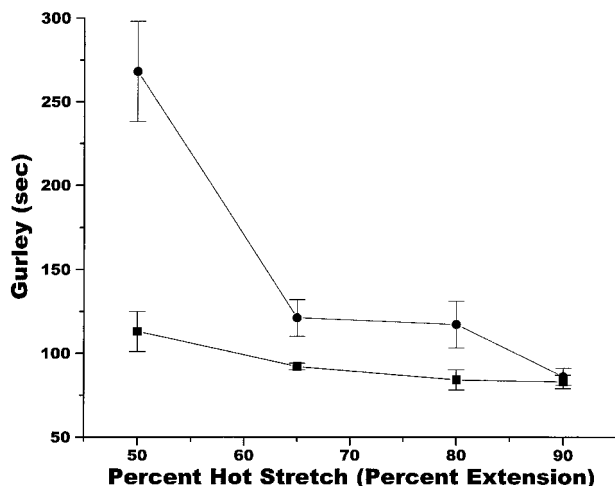


**Figure 18** Effect of the hot stretch parameters ( $T_{hs}$  and %HS) on the Gurley number for F1 stretched films (■)  $T_{hs} = 100^\circ\text{C}$  and (●)  $T_{hs} = 115^\circ\text{C}$ . The remainder of the main anneal/stretching condition were kept intact.

uniaxial tension at lower annealing temperatures was found to produce interlamellar voids on the order of nanometers in size, as viewed by AFM. Thus, the main deformation process appeared to be lamellar separation. These findings were further supported by the use of SAXS on these samples, where a long spacing of ca. 13–14 nm was measured. Upon increasing the isothermal annealing temperature above  $130^\circ\text{C}$ , the long spacing values for the films annealed under tension were similar to those observed for free-annealed specimens. Additionally, as the specific tension level utilized during annealing was increased, the scattering intensity  $[I(s)]$  of the first-order peak (meridonal position) for the corresponding sample diminished but did not shift with respect to  $s$  (i.e.,  $s^*$  did not change). These results suggest that the lamellae were possibly tilted away from the MD

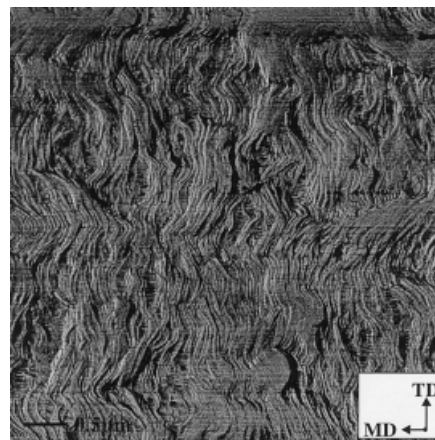


**Figure 19** AFM phase image of the F1 stretched film F1- $T_a$ 110C,  $T_{hs}$ 145C displaying the effect on microporosity when  $T_{hs} > T_a$ . The MD is labeled, and the image is  $5 \times 5 \mu\text{m}$ .

but still retained their dimensions. This conclusion is based upon previous studies regarding the deformation behavior POM spherulitic morphologies<sup>14</sup> as well as the earlier AFM results. In the present samples, lamellar tilting was observed via AFM for any annealed sample as long as elevated temperatures ( $T_a \geq 130^\circ\text{C}$ ) with higher tension levels (ca. 9–15%) were utilized. Further discussion of the SAXS results for the free-annealed specimens will be given later. Lamellar separation was, therefore, not the main deformation mode upon the application of higher tension levels ( $\geq 3\%$ ) at higher annealing temperatures ( $T_a \geq 130^\circ\text{C}$ ). Instead, inter- and intralamellar slip as well as shear appears to be the main deformation modes accounting for the lamellae tilting.

The transition between different deformation modes with draw is not necessarily a novel finding for POM. O'Leary and Geil<sup>14</sup> previously re-

**Table VII** The Gurley Number Results from Membranes of Different %HS and  $T_{hs}$  Combinations: All Other Annealing/Stretching Parameters Remained Constant with the Standard Condition

$T_{hs}$ ( $^\circ\text{C}$ )	%HS (% Extension)			
	50	65	80	90
85	$357 \pm 5$ s	$271 \pm 21$ s	$113 \pm 4$ s	$98 \pm 15$ s
100	$113 \pm 12$ s	$92 \pm 2$ s	$84 \pm 6$ s	$83 \pm 4$ s
115	$132 \pm 15$ s	$112 \pm 11$ s	$95 \pm 5$ s	$86 \pm 5$ s
130	$541 \pm 91$ s	$478 \pm 83$ s	$394 \pm 43$ s	$345 \pm 20$ s
145	$\geq 1000$ s	$\geq 1000$ s	$\geq 1000$ s	$\geq 1000$ s



**Table VIII The Gurley Number Results from F1 Microporous Films That Were a Product of Different %CS and %HS Combinations**

%HS (% Extension)	%CS (% Extension)		
	50	70	90
50	100%	120%	140%
	113 ± 12 s	96 ± 4 s	90 ± 5 s
65	115%	135%	155%
	92 ± 2 s	89 ± 7 s	78 ± 3 s
80	130%	150%	170%
	84 ± 6 s	82 ± 2 s	69 ± 4 s
90	140%	160%	180%
	83 ± 4 s	76 ± 3 s	63 ± 3 s

The %TS is displayed in the top left corner of each cell. The other annealing/stretching parameters remained constant with the standard condition.

ported deformation results with respect to POM materials possessing quiescently crystallized spherulitic morphologies. However, analogies can be drawn between their results and the stacked lamellae morphologies presented here. Specifically, comparisons can be made in the equatorial spherulitic regions, where the lamellae are stacked with their long directions perpendicular to the draw direction. In these regions, the lamellae should behave similar to our stacked lamellar morphologies. In fact, it was the equatorial regions that the following observations of O’Leary and Geil addressed. In their report, they noted that the transition from void formation to no void formation with draw occurred at a temperature of approximately 130°C using a rate ca. 5 mm/min. Below 130°C, these authors noted that voids formed in regions where the deformation was perpendicular to the lamellae, while above this temperature voids did not occur. Structurally, at elevated temperatures (>130°C), the long direction of the lamellae in these equatorial regions tilted towards the draw direction with increasing draw. In fact, the lamellae were observed to preferentially tilt approximately 30° into the draw direction. From this, they concluded that the chain axes within the lamellae lie at roughly this same angle to the lamellae normal (30°). They also reported that the lamellar tilting is further accompanied by lamellar breakup into slightly smaller units that are still much larger than any fibrillar-like structures.

The findings of O’Leary and Geil are also helpful to explain the effect of tension on the “c” and

“a”-axis orientation along MD. The reader may recall, that as the specific tension level increased, the corresponding “c” and “a”-axis orientations along MD decreased. In fact, the latter was absent in samples annealed under 15% tension. O’Leary and Geil further suggested that inter- and intralamellae slip occurs along the chain axis, specifically along the (100) slip plane. They also proposed that as the deformation level increased, the twisting period decreased for lamellae at right angles to the draw direction. Eventually, lamellar discontinuities (i.e., lamellar fracture) were produced at sufficiently high deformation levels where the lamellae fracture in a twisted portion. Thus, smaller lamellae were produced essentially absent of twisting.<sup>15</sup> This explanation may account for our observed loss of

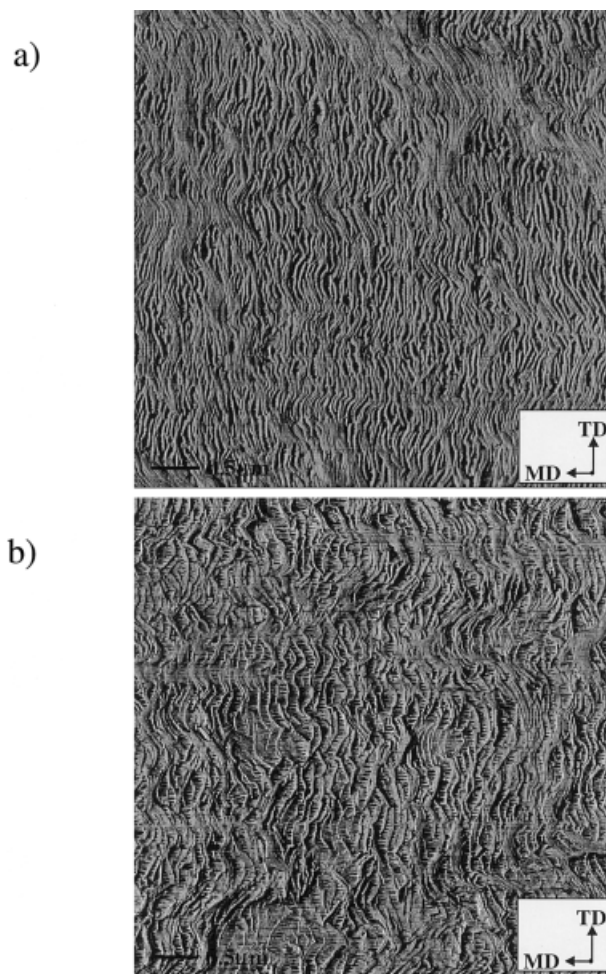


**Figure 20** AFM phase images displaying the influence of %TS on F1 membrane morphology: (a) %TS = 100%, and (b) %TS = 180%. The MD is labeled, and the images are each 5 × 5 μm.



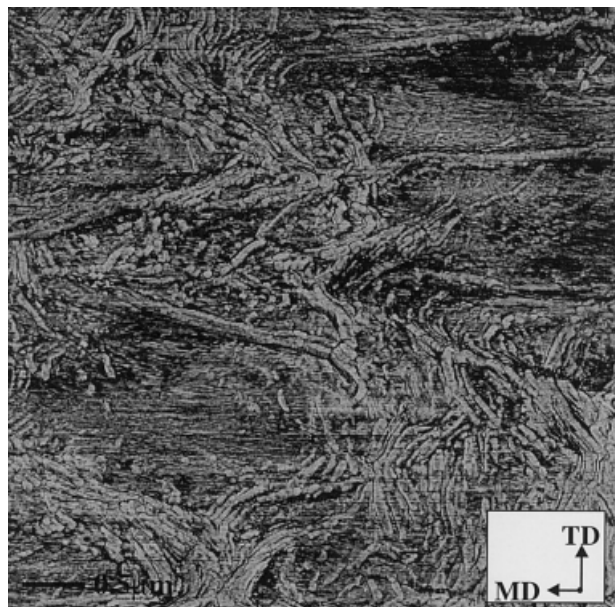


**Figure 21** AFM phase image of the D1 stretched film utilizing the standard annealing/stretching condition. The MD is labeled, and the image is  $5 \times 5 \mu\text{m}$ .

“a”-axis orientation along MD at higher tension levels (recall Fig. 11). The chains that composed these twisted portions initially contribute to the decrease in  $f_c$  orientation, i.e., decreased azimuthal dependence of the (100) reflection. Additionally, it is probable that many chains within the tilted lamellae are still parallel to the lamellar normal given the low levels of extension utilized. Such a result would further contribute to the decrease in the crystal orientation. It is speculated, however, that for greater levels of draw than those investigated here, the chains might well be sufficiently realigned with the MD to produce a higher WAXS azimuthal dependence than we observed.

A number of these morphological and structural results are a consequence of an  $\alpha_c$  relaxation present in POM. Recall that the range of temperatures encompassing the resin F  $\alpha_c$  relaxation, as measured via DMA at 1 Hz, occurs over the range of 40–165°C. Thus, as the annealing temperature increased from 85 to 150°C, the  $\alpha_c$  relaxation was more activated. Upon applying tension at the higher annealing temperatures, the polymer chains were better able to translate through the crystal more readily. The result is that at the lower temperature of 110°C, the lamellae behaved more solid-like (less chain slippage through the lamellae), and thus the main deformation mode was lamellar separation, rather than chain

slip with lamellar tilting. The end result was more pores and less of a change in  $f_c$  vs. films annealed at 145°C under tension.

The presence of an  $\alpha_c$  relaxation in POM also accounts for the  $X_c$  increase and  $\Delta w$  decrease as annealing time or temperature was increased. In fact, similar findings for other polymers possessing an  $\alpha_c$  relaxation<sup>6,15–17</sup> have been observed. Also recall the  $T_m$  was not systematically affected, while the annealing temperature and time did influence the long spacing. In conclusion, with regard to the annealing behavior of POM, the time spent in the range of temperatures encompassing the POM  $\alpha_c$  relaxation and the temperature at which this time is spent are two factors that influence the resulting  $X_c$ ,  $\ell$ , and  $\Delta w$ .

We postulate that a more uniform and thicker crystalline phase, as a result of higher annealing temperatures and/or long annealing times, translates into a more permeable stretched film with higher observable amounts of microporosity. However, if the annealing temperature becomes too high (150°C), permeability begins to decrease. It is speculated that this possibly is a result of macroscopic lamellar melting during annealing, which would not be beneficial to lamellar splaying upon stretching. This was supported by Figure 22, an AFM micrograph of a free-annealed F1 film using  $T_a$  equal to 150°C for 20 min, where partial

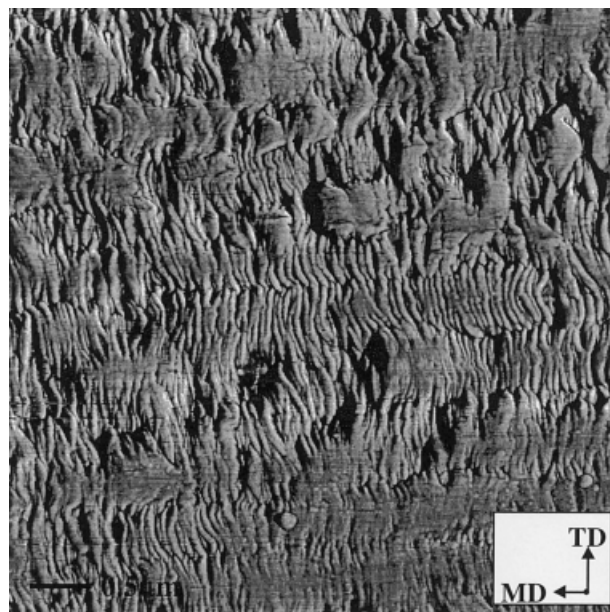


**Figure 22** AFM phase image of the F1 free-annealed film utilizing a  $T_a = 150^\circ\text{C}$  for 20 min. The MD is labeled, and the image is  $5 \times 5 \mu\text{m}$ .

lamellar melting was recognized on the film surface. Because there is only a small difference in membrane permeability for stretched films annealed at 145°C vs. 150°C for similar stretching conditions, the surface melting effect is not large.

For the production of microporous films utilizing the MEAUS process, the desired deformation mode during stretching (third stage) is lamellar splaying (separation). According to Peterlin and coworkers,<sup>18</sup> this mode is initially the result of ductile drawing between the crystalline lamellae in the disordered amorphous phase using a slow strain rate and sufficient temperature. Thus, the cold stretch temperature must be sufficiently high to provide enough thermal energy enabling cooperative segmental mobility within the *amorphous* phase. Precisely, this temperature ( $T_{cs}$ ) must be greater than the  $T_g$  for a specific polymer. In the case of POM, the glass transition temperature is disputed within the literature,<sup>15</sup> however, both temperatures (ca. 0 and -70°C) thought to be attributed to  $T_g$  occur below room temperature. For all the temperatures utilized here during cold stretching, sufficient *amorphous* mobility should therefore be achieved. However, it is speculated that at the high levels of crystallinity present in the POM annealed films, higher  $T_{cs}$  values are required to provide adequate mobility for the initial ductile drawing of the amorphous phase. Why then does the permeability decrease for membranes cold stretched at 70°C vs. those stretched at 50°C? This is attributed to higher *crystalline* mobility, which is more activated at 70°C vs. 50°C. Thus, the lamellae behave less solid-like with greater chain translation occurring,<sup>6</sup> resulting in less micropore nucleation at the higher temperature.

In contrast to the cold stretching step, chain slippage is exactly the desired outcome in hot stretching, which is facilitated by a sufficiently high temperature during this step. For the resin F films, a hot stretch temperature of 100°C produced the lowest final film permeability. The reader may recall that the stretched film permeability levels decreased if the hot stretch temperature was increased above this value. Thus, during hot stretching at elevated temperatures ( $\geq 130$ ), there is likely too much crystalline mobility and crystalline melting is occurring. However, these explanations are pure conjecture as there is no direct evidence.

The explanation accounting for the permeability and observable pore size dependence on the percent cold or hot stretch is quite evident. Larger

cold stretch extension levels “nucleate” greater numbers of pores that become enlarged during hot stretching as the extension level is increased. This also translates into larger percent total stretch values producing more permeable membranes with larger micropores as was observed in Figure 20. As previously discussed, cold and hot stretching must be executed at the proper temperatures to produce the desired outcome. From the above results and discussion, the general film permeability dependence on the annealing and stretching parameters was recognized. In fact, a resin F final film possessed the highest permeability if it was free-annealed at 145°C for 20 min. followed by cold stretching at a temperature of 50°C to 90% extension and then hot stretched at 100°C to an extension level of 90%. Even when the Gurley values were normalized to final film thickness, this result still held.

The effect of precursor  $f_c$  and morphology has yet to be discussed, although it was found to influence the membrane permeability. Specifically, it was discovered that a F1 stretched sample possessed a higher permeability than a F2 final film, when annealed and stretched under equal conditions. Recall that precursor F1 was characterized by a slightly more planar lamellar morphology and a higher  $f_c$  value with respect to the MD than the precursor F2 (0.81 vs. 0.75, respectively). Therefore, starting film morphology and orientation state play an integral role on the final film properties. In most cases upon annealing and stretching the resin F precursors, microporous membranes were produced, although to varying degrees for the processing window studied. This was not true for resin D films, which were also subjected to a large number of variable combinations similar to those applied to the resin F films. Once again, it was the precursor morphology that is believed to be the cause. The reader may recall that precursor D1 possessed a sheaf-like twisted lamellar morphology with an  $f_c$  equal to 0.45.

From the above results and discussion, the criteria or recommended prerequisites by the authors for successfully converting a semicrystalline polymer by the MEAUS process into a microporous membrane appear to be correct. Reiterating, these prerequisites are: (1) “fast” crystallization kinetics; (2) a highly planar lamellae morphology (limited lamellar twisting) for the extruded precursor; (3) “high” orientation of the crystalline phase in the precursor; (4) proper film thickness (1 mil) and quenching rate to facilitate

rapid heat transfer of the film to limit skin-core effects; and (5) presence of a  $\alpha_c$  relaxation.

Lastly, the annealing and stretching conditions must be optimized to attain the best permeability as has been shown for these POM films for the processing conditions studied.

## CONCLUSIONS

This particular article addressed the findings of the latter two stages (annealing and stretching) regarding the MEAUS process utilizing resins D and F. In terms of the effects of annealing temperature and time on the films, the following conclusion can be made. As the values of  $T_a$  or  $t_a$  were increased, the magnitude of  $X_c$  and long spacing increased, which is attributed to the presence of crystalline mobility, associated with the  $\alpha_c$  relaxation. The application of tension during annealing influenced whether the annealed film morphology did or did not possess voids, which also depended upon the annealing temperature utilized for tension levels greater than 3%.

The morphological alterations as a result of annealing impacted the final microporous morphology. Greater tension levels produced lower permeability as well as less typical porous morphologies, regardless of the other annealing or stretching conditions utilized. In contrast, greater membrane permeability was obtained when higher values of  $T_a$  and  $t_a$  were employed during annealing. The final film permeability also increased for greater extension levels during either the cold or hot stretching steps. Additionally, the stretching temperature ( $T_{cs}$  or  $T_{hs}$ ) affected the microporosity and permeability. The initial melt-extruded morphology and  $f_c$  were also found to be very influential regarding the microporosity and permeability of the final film. In fact, the lower  $f_c$  value and slightly twisted lamellar morphology are believed to be the main reason why the precursors from resin D were not able to form microporous membranes.

The authors would like to thank the Celgard Corporation LLC for their continuing financial assistance for this project as well as the informative discussions that have taken place with them. Also, the authors thank Stephen McCartney for aiding in the instruction of AFM.

## REFERENCES

1. Johnson, M. B.; Wilkes, G. L. *J Appl Polym Sci*, to appear.
2. Johnson, M. B.; Wilkes, G. L. *J Appl Polym Sci* 2002, 83, 2095.
3. Johnson, M. B.; Wilkes, G. L. *J Appl Polym Sci* 2001, 81, 2944.
4. Druin, M. L.; Loft, J. T.; Plovan, S. G. U.S. Pat. 3,801,404, assigned to Celanese Corp.
5. Boyd, R. H. *Polymer* 1985, 26, 323; 1985, 26, 1123.
6. Rault, J. *JMS-Rev Macromol Chem Phys* 1997, C37, 335.
7. Marand, H.; Xu, J.; Srinivas, S. *Macromolecules* 1998, 31, 8219.
8. Garber, C. A.; Clark, E. S. *J Macromol Sci Phys* 1970, B4, 499; *Int J Polym Mater* 1971, 1, 31.
9. Quynn, R. G.; Brody, H. *J Macromol Sci Phys* 1971, B5, 721.
10. Odian, G. *Principles of Polymerization*; John Wiley & Sons: New York, 1991, 3rd ed.
11. Hermans, P. H.; Hermans, J. J.; Vermaas, D.; Weidinger, A. *J Polym Sci* 1947, 3, 1.
12. Yu, T. H. Ph.D. Dissertation (advisor: G. L. Wilkes), Virginia Tech, 1995.
13. Celgard Corporation LLC, Company product literature.
14. O'Leary, K.; Geil, P. H. *J Macromol Sci Phys* 1968, B2, 261.
15. McCrum, N. G.; Read, B. E.; Williams, G. *Anelastic and Dielectric Effects in Polymeric Solids*; Wiley: New York, 1967.
16. Popli, R.; Mandelkern, L.; Bersion, R. S. *J Polym Sci Polym Phys Ed* 1984, 5, 407.
17. Zhou, H.; Wilkes, G. L. *Macromolecules* 1994, 30, 2412.
18. Peterlin, A.; Sakaoku, K. *J Appl Phys* 38, 1967, 4152.